engineering proceedings

MDPI

Proceedings

Electrical Characterization of Hydrothermally Synthesized Manganese Dioxide Nanowires with Regard to NO_2 Adsorption/Desorption Thermodynamics

Petr Smisitel [1,*], Helena Simunkova [1,2,*], Ondrej Chmela [1,2], Martha Claros [3], Stella Vallejos [4] and Jaromir Hubalek [1,2]

[1] Central European Institute of Technology (CEITEC), Brno University of Technology, Czech Republic, Purkynova 656/123, 612 00 Brno, hubalek@vutbr.cz
[2] Department of Microelectronics, Faculty of Electrical Engineering and Communication (FEEC), Brno University of Technology, Czech Republic, Technicka 3058/10, 616 00 Brno
[3] Escuela de Ingeniería Química, Pontificia Universidad Católica de Valparaíso, Valparaíso, Chile, Av Brasil 2950, Valparaíso, martha.claros@pucv.cl
[4] Instituto de Microelectrónica de Barcelona, IMB-CNM (CSIC), Cerdanyola del Vallès, Spain, 08193 Cerdanyola del Vallès, Barcelona, stella.vallejos@imb-cnm.csic.es
* Correspondence: smisitel@vutbr.cz (P.S.); simunkova@vutbr.cz (H.S.); Tel.: +420541146392 (H.S.)
† Presented at CSAC2023: The 2nd International Electronic Conference on Chemical Sensors and Analytical Chemistry, online, 16–30 September 2023.

Abstract: Self-assembled MnO_2 nanowires were hydrothermally synthesized and electrically characterized in different ambiences. The nanowires were approximately 3-10 μm long and about 20-100 nm in diameter. Single nanowires were aligned perpendicularly across two parallel gold electrodes transducer by means of dielectrophoresis (DEP) technique. Resistivity changes in synthetic air, nitrogen, and NO_2 were tested in a range from 100 °C up to 300 °C. The resistivity changes were observed accounting for oxygen reduction on the NWs surface as the electrons were moving from the NWs to the oxygen. The resistivity was explored at a constant current arrangement test. Based on resistivity changes, electrical properties, such as, activation energy and a type of semiconductor, were estimated.

Keywords: gas sensing; nanowires; manganese dioxide; nitrogen dioxide; Arrhenius plot; defect structure; ion mobility; variable oxidation state; structural instability

Citation: Smisitel, P.; Simunkova, H.; Chmela, O.; Claros, M.; Vallejos, S.; Hubalek, J. Electrical Characterization of Hydrothermally Synthesized Manganese Dioxide Nanowires with Regard to NO_2 Adsorption/Desorption Thermodynamics. **2023**, *4*, x. https://doi.org/10.3390/xxxxx

Academic Editor(s):

Received: date
Accepted: date
Published: date

Publisher's Note: MDPI stays neutral with regard to jurisdictional claims in published maps and institutional affiliations.

1. Introduction

Manganese, a transition metal, can form a range of semiconducting oxides with oxidation state from +2 to +7. Manganese dioxide is a suitable candidate in photo-catalysis, sensors, supercapacitors, etc., with different crystalline phases like α-MnO_2, β-MnO_2, γ-MnO_2 and δ-MnO_2 [1]. Diverse deposition techniques of nanostructured MnO_2, such as, plasma-enhanced chemical vapor deposition (PE-CVD) [2], electrochemical deposition [3] or hydrothermal deposition [4] are known. Although, MnO_2 is abundant, low cost and environmentally friendly semiconductor, only a limited number of reports were dedicated to manganese dioxide gas sensors. Resistive MnO_2 response towards, e.g., ethanol [1, 5], NH_3 [6, 7], H_2 or warfare agents [8, 9] adsorption/desorption was tested. Only few studies have been conducted recently regarding MnO_2 as a NO_2 chemoresistive sensor, e.g.: [3, 10]. The NO_2 detection limit was 5 ppm [3]. Herein, hydrothermally prepared single standing α-MnO_2 nanowires (NWs) were tested for the first time on their resistivity changes upon NO_2 gas adsorption/desorption processes. Analyzed concentration range was 0.1 to 11 ppm. Temperature sensing range was 100-300 °C at the concentration of 11 ppm NO_2 in synthetic air (SA).

2. Materials and methods

2.1. Sample preparation and stabilization

MnO_2 NWs (about 3-10 μm long and about 20-100 nm wide) were prepared hydrothermally according to our previous study by Claros *et al.* [11]. Comparing X-ray diffraction (XRD) peaks and ICDD card No. (44-0141) of our MnO_2 NWs with XRD pattern and ICDD card number collected by Wang and Li [4], α-phase might be attributed to our MnO_2 NWs. Brown NWs powder was suspended in water and redeposited by dielectrophoresis [12] on two parallel gold electrodes having separation distance of 4 or 6 μm. Single nanowires standing perpendicularly to the electrodes were observed by scanning electron microscopy (SEM), whereas large bunches were removed by focused ion beam. These sensor chips were characterized in a test chamber (140 cm^3 volume) at constant gas flow. A heater with thermocouple was used to control the temperature and constant current was applied to the NWs (Keithley 2401 SourceMeter) to monitor the resistance. The NWs response to NO_2 gas ambient was tested at diverse temperatures and concentrations. The measurements were performed on two diverse samples with 1 or 3 MnO_2 NWs. The entire cross-sectional area was $9.5 \cdot 10^{-3}$ μm^2 or $98.2 \cdot 10^{-3}$ μm^2, respectively. The NW´s length was about 4 or 6 μm, equal to the gold electrodes gap. The nanowires were initially stabilized at 300 °C for 3 hours at potential up to 0.5 V under synthetic air (SA) flow 50 sccm.

2.2. Thermal resistivity analysis

After the initial stabilization a sample with one MnO_2 NW was tested under low constant SA flow (50 sccm) and constant probing current 10 nA. Temperature was set from 25 °C to 300 °C with 10 °C increment in 5 minutes. Afterwards, the test chamber was purged with N_2 for 24 hrs at 250 °C followed by 10 hrs at room temperature to remove oxygen and stabilize the sample. The entire cross-sectional area was $9.5 \cdot 10^{-3}$ μm^2.

2.3. NO_2 thermal analysis

Sensor resistivity response to NO_2 gas (11 ppm in SA) was tested at five different temperatures 100-300 °C at constant current 20 nA and constant gas flow 200 sccm. The sensor response was defined as $R = R_{SA}/R_{NO2}$ where R_{NO2} is the sensor resistance after NO_2 exposure and R_{SA} represents the sensor resistance baseline. The baseline was average of 5 last minutes before first NO_2 exposure obtained at pure SA and given temperature (100-300 °C). The baseline differed with each temperature, and it was defined after 30 minutes SA purge (200 sccm) at given temperature. Among the five temperature steps, there was always additional stabilization under SA flow at 250 °C for 40 minutes due to baseline fluctuations and to desorb NO_2 from the sensor which would be slow at low temperatures. Response was further evaluated at 5 to 30 minutes after the start of the exposure. Each NO_2 gas exposure took 30 minutes. The sensor cross-sectional area was $98.2 \cdot 10^{-3}$ μm^2.

2.4. NO_2 concentration analysis

The sample with three MnO_2 NWs was tested at diverse NO_2 concentrations obtained by mixing pure synthetic air (SA) and NO_2 (11 ppm in SA) gas. The NO_2 concentration was set from 0.1 ppm in SA up to 10 ppm in SA. The sensor cross-sectional area was $98.2 \cdot 10^{-3}$ μm^2. Before the initial NO_2 exposure, the sample was further stabilized at the working temperature 250 °C for 30 minutes and pure SA flow (200 sccm). The NO_2 concentration was increased at every exposure step from 0.1 ppm up to 10 ppm. A constant NO_2 flow of 200 sccm for 10 minutes was set at each step. After each exposure the sensor was purged by pure SA (200 sccm flow) for 110 minutes. Sensor response and recovery were evaluated. As the baseline shift could not be neglected, the baseline R_{SA} was determined newly before each NO_2 pulse. The baseline was average resistance of 5 last minutes before every NO_2 exposure pulse.

3. Results and discussion

3.1. Thermal resistivity analysis

The thermal analysis in a range 25-300 °C was measured in SA and N_2, see Figure 1. In standard semiconductor, the free charge carriers are thermally activated meaning the resistivity should follow (if other effects are negligible) the equation:

$$\rho = \rho_0 \, e^{E_a/kT} \quad (1)$$

where ρ is the resistivity, ρ_0 a material constant, E_a activation energy and k is Boltzmann constant. If this simple equation fits the measured data, then the sensor behavior would be well predictable. In SA, the data fit well up to 220 °C with activation energy 0.2 eV. Above 220 °C the resistivity starts to deviate from the exponential fit and increases. In nitrogen, the resistivity deviates from the fit above 150 °C and starts to decrease. Under N_2, the activation energy was 0.16 eV in the temperature range 25-150 °C and 0.31 eV in 150-300 °C. P-type semiconductive sensors have lower resistivity in O_2 compared to N_2 ambient. It is generally explained by formation of positively charge accumulation layer (holes accumulation) under the surface where oxygen adsorbs. In some studies, MnO_2 oxides were classified as p-type [13], in other studies as n-type semiconductors [9]. We might presume that both types of the semiconductive behavior might be possible under certain circumstances. In our previous study [12] we had determined that 24 single standing MnO_2 NWs behaved as p-type semiconductor. However, the number of NWs tested in present study is 24 times lower than in that work. Moreover, our recent impedance and Mott-Schottky analyses made on one single standing NW determined that both types of semiconductive behavior are possible at low frequency range. According to our previous X-ray photoelectron spectroscopy (XPS), the bonding energies in the MnO_2 NWs indicate mainly Mn (IV) oxidation state with low contribution of Mn (III) [11]. Bonds, such as Mn-O-Mn, Mn-O-H, or H-O-H were determined in our NWs by that study. Moreover, it was published elsewhere that among the structural polymorphs, the α (our case) and δ phases exhibit a strongly mixed valent character, with Mn^{3+} defects being common throughout the structure [14]. Mn^{3+} defects make it more likely that ionic oxygen species (O^-, O_2^-, O^{2-}) and hydroxyl groups (OH), will form on the MnO_2 surface and react with NO_2 [3].

Under N_2 ambient the activation energy below and above 150 °C was different. The reason is not clear, possibly some structural changes might occur due to the current flow in conjunction with the high temperature as the MnO_2 is very active material and structural changes are known. For example, Bailey [15] reviewed that MnO_2 exists in variety structural forms, which include cation vacancies, lower valent manganese ions (particularly Mn^{3+}), structural water (present as protons to accommodate absent of lower valent manganese species [16-18]), and possibly microtwinning [19], although there is still debate as to its presence [20]. Donne *et al.* [21] published, that position of individual ionic species, such as Mn^{4+}, Mn^{3+}, O^{2-}, OH^- within the MnO_2 crystal lattice is not fixed, with proton and electron movement tending towards a homogeneous distribution. Therefore, we think that elevated ionic and defect mobility in the MnO_2 structure especially at high temperatures might possibly switch the semiconductor type behavior. A possible surface reaction of Mn^{3+} with oxygen might lead to the resistivity sudden increase above 220 °C in the O_2 ambient, see Figure 1.

Additionaly, Iwamoto *et al.* [22] determined that a large amount of oxygen is adsorbed in MnO_2 structure related to its low stability associated with redox reactions promoted by variable oxidation states. In general, the unexpected behavior of this type of sensor might be given by its low structural stability.

Additionally, the NW cannot be held at high temperatures (above 250 °C) for more than approximately 40 minutes as it leads to irreversible rapid increase of the resistivity up to unmeasurable values, even though the sample has not shown any damage by SEM imaging. This was the case only during N_2 purge, not under SA or NO_2 ambient.

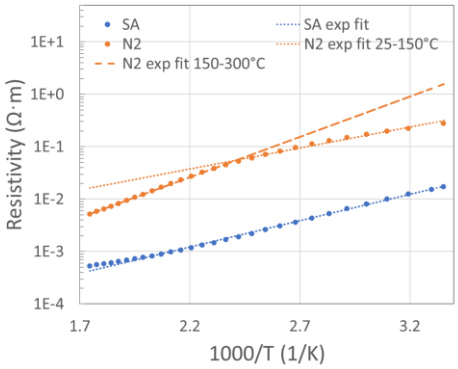

Figure 1. Arrhenius plot of resistivity vs. temperature range 25 – 300 °C fitted to equation (1).

3.2. NO_2 thermal analysis

NO_2 gas sensing (11 ppm) of three MnO_2 nanowires at diverse temperatures is shown in Figure 2. We see the thermal activation of response, which is typical for metal oxide semiconductive sensors. The response increases with temperature. However, in our case, a deviation from that behavior occurred at 300 °C as the initial resistivity decrease (typical for p-type behavior) was followed up with unexpected resistivity increase after about 10 minutes of NO_2 exposure. Again, some structural changes at 300 °C might be a reason for this phenomenon. The sensor response to 11 ppm NO_2 reached its maximum at 250 °C, being almost 1.07. Baseline resistivity instabilities (especially unexpected and random resistivity increase in SA at 200 and 300 °C) might indicate the structural changes too. It was not possible to propelly evaluate the recovery process due to the baseline instabilities however it seems that after 30 min exposure to NO_2 the 30 min purge by SA migt not be long enough.

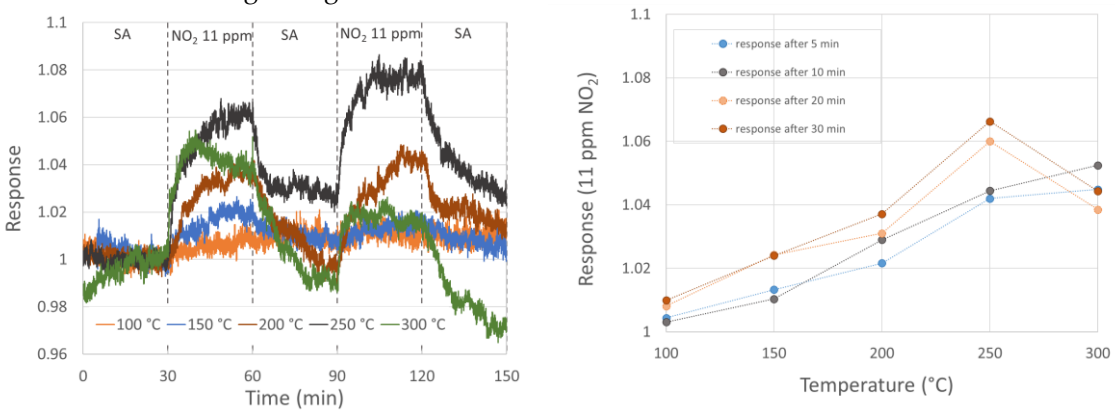

(**a**) (**b**)

Figure 2. Sensor response to 11 ppm NO_2 at diverse temperatures: (**a**) Sensor response with 30 minutes NO_2 exposure and 30 minutes SA purge; (**b**) Sensor response after 5, 10, 20 and 30 minutes NO_2 exposure.

3.2. NO_2 concentration analysis

Response of three single standing MnO_2 NWs to NO_2 gas at diverse concentration was studied, see Figure 3. To increase the signal to noise ratio the probing current was raised to 100 nA. The response had growing trend up to 4 ppm concentration followed by almost random value around 1.04 up to 10 ppm concentration, Figure 3 (b). Despite the low responsivity when compared to alternate sensors, e.g. WO_3 based, the signal to noise ratio allows to detect NO_2 clearly already at 2 ppm with response 1.02 at 250 °C. Figure 3 (a) shows the response within 10 minutes exposure followed by 110 minutes of SA purge.

Up to about 8 ppm NO_2 the baseline resistivity increased rapidly without any hint of returning to the initial value. As this phenomenon would further complicate the NO_2 detection at low concetrations, conditions under which the baseline stabilizes should be further tested. Recovery in our experiment was estimated only at two concentrations with more or less stable baseline (2 and 9 ppm NO_2), see Figure 4.

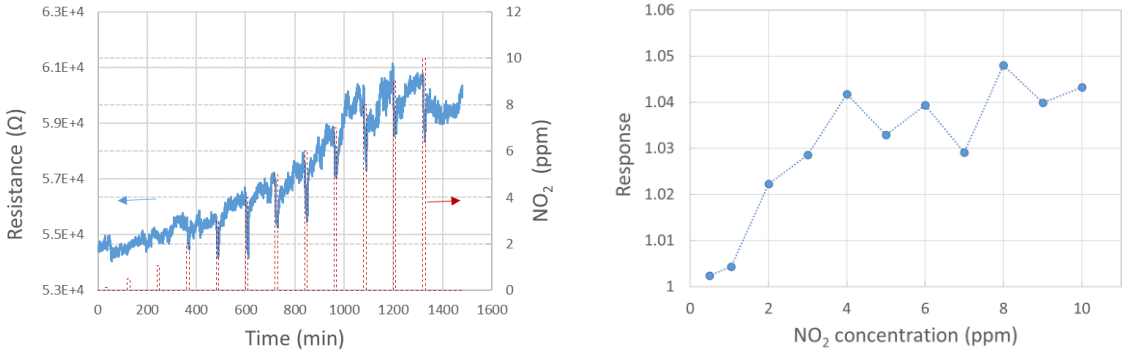

(**a**) (**b**)

Figure 3. Sensor response at 250°C to diverse NO_2 concentrations: (**a**) 10 min NO_2 exposure followed by 110 min pure SA purge; (**b**) Response to NO_2 after 10 min exposure.

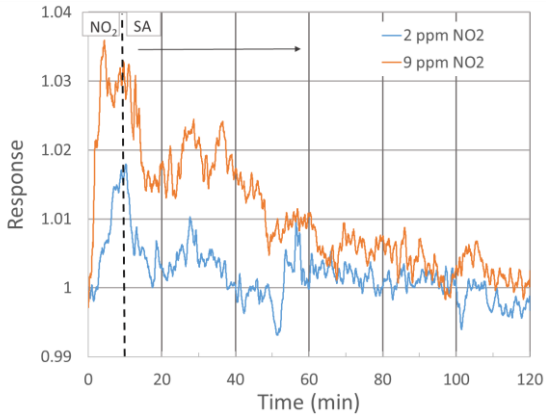

Figure 4. Sensor response during recovery in pure SA over 110 minutes after 10 min exposure to 2 and 9 ppm NO_2 gas.

4. Conclusions

Single standing MnO_2 nanowires revealed low stability during the resistive sensing experiments. The resistivity fluctuations might be caused be structural changes because of high ionic and defect mobilities. Conditions under which the baseline stabilizes should be further tested. Sensor response at 250 °C varied from 1.02 up to 1.07 approximately for 2 ppm and 11 ppm of NO_2, respectively.

Author Contributions: Conceptualization, H.S. and P.S.; methodology, P.S. and H.S. formal analysis, P.S. and H.S.; investigation, H.S. and P.S.; resources, O.Ch. and M.C. writing—original draft preparation, H.S. and P.S.; writing—review and editing, S.V. and P.S.; visualization, H.S.; funding acquisition, J.H. All authors have read and agreed to the published version of the manuscript."

Funding: The work was done under the Czech Grant Agency project no. 22-14886S. CzechNanoLab project LM2023051 funded by MEYS CR is gratefully acknowledged for the financial support of the sample fabrication at CEITEC Nano Research Infrastructure.

Conflicts of Interest: The authors declare no conflict of interest.

References

1. Umar, A., Ibrahim, A.A., Kumar, R., Albargi, H., Zeng, W., Alhmami, M.A.M., Alsaiari, M.A., Baskoutas, S. Gas sensor device for high-performance ethanol sensing using α-MnO2 nanoparticles. Mater. Lett. **2021**, *286*, 129232, https://doi.org/10.1016/j.matlet.2020.129232.
2. Barreca, D., Gasparotto, A., Gri, F., Comini, E., Maccato, C. Plasma-assisted growth of β-MnO_2 Nanosystems as Gas Sensors for Safety and Food Industry Applications. *Adv. Mater. Interfaces* **2018**, *5*, 1800792. https://doi.org/10.1002/admi.201800792.
3. Pedowitz, M.D., Kim, S., Lewis, D.I., Uppalapati, B., Khan, D., Bayram, F., Daniels, K.M. Fast selective sensing of nitrogen-based gases utilizing δ -MnO_2-epitaxial graphene-silicon carbide heterostructures for room temperature gas sensing. *J. Microelectromech Syst.* **2020**, 1–7. doi:10.1109/jmems.2020.3007342.
4. Wang, X., Li, Y. Selected-control hydrothermal synthesis of α- and β-MnO_2 single crystal nanowires. *J. Am. Chem. Soc.* **2002**, *124*, 12, 2880–2881. https://doi.org/10.1021/ja0177105.
5. C. Liu, C., Navale, S.T., Yang, Z.B., Galluzzi, M., Patil, V.B., Cao, P.J., Mane, R.S., Stadler, F.J. Ethanol gas sensing properties of hydrothermally grown a-MnO_2 nanorods, *J. Alloys Compd.* **2017**, *727*, 362–369. https://doi.org/10.1016/j.jallcom.2017.08.150.
6. Zhang, W., Zeng, C., Kong, M., Pan, Y., Yang, Z. Water-evaporation-induced self-assembly of a-MnO_2 hierarchical hollow nanospheres and their applications in ammonia gas sensing, *Sens. Actuators B Chem.* **2012**, *162*, 1, 292–299. https://doi.org/10.1016/j.snb.2011.12.080.
7. Sovizi, M.R., Mirzakhani, S. Highly sensitive detection of ammonia gas by 3D flower-like γ-MnO_2 nanostructure chemiresistor, *J. Taiwan Inst. Chem. Eng.* **2020**, *111*, 293–301. https://doi.org/10.1016/j.jtice.2020.04.017
8. Xiao, J.; Liu, P.; Liang, Y.; Li, H.B.; Yang, G.W. High aspect ratio β-MnO2 nanowires and sensor performance for explosive gases. *J. Appl. Phys.* **2013**, *114*, 073513. https://doi:10.1063/1.4819218
9. Bigiani, L., Zappa, D., Maccato, Ch., Comini, E., Barreca, D., Gasparotto, A. Quasi-1D MnO_2 nanocomposites as gas sensors for hazardous chemicals. *Appl. Surf. Sci.* **2020**, *512*, 145667. https://doi.org/10.1016/j.apsusc.2020.145667.
10. Shinde, P.V., Xia, Q.X., Ghule, B.G., Shinde, N.M., Seonghee, J., Kim, K.H., Mane, R.S. Hydrothermally grown α-MnO_2 interlocked mesoporous micro-cubes of several nanocrystals as selective and sensitive nitrogen dioxide chemoresistive gas sensors. *Appl. Surf. Sci.* **2018**, *442*, 178-184. https://doi.org/10.1016/j.apsusc.2018.02.144.
11. Claros, M., Kuta, J., El-Dahshan, O. Michalička, J., Jimenez, Y.P., Vallejos, S. Hydrothermally synthesized MnO_2 nanowires and their application in Lead (II) and Copper (II) batch adsorption. *J. Mol. Liq.* **2021**, *325*, 115203. https://doi.org/10.1016/j.molliq.2020.115203.
12. Smisitel, P., Simunkova, H., Chmela, O., Claros, M., Vallejos, S., Hubalek, J. Electrical characterization of hydrothermally synthesized metal oxide nanowires with regard to oxygen adsorption/desorption thermodynamics. In Proceedings of 14th International Conference on Nanomaterials, NANOCON 2022, Brno, Czech Republic, 19.-21. October 2022, pp. 64-70. https://doi:10.37904/nanocon.2022.4583.
13. Kim, H.-J., Lee, J.-H. Highly sensitive and selective gas sensors using p-type oxide semiconductors: Overview. *Sens. and Actuators B Chem.* **2014**, *192*, 607-627. https://doi.org/10.1016/j.snb.2013.11.005.
14. Julien, C.M., Massot, M., Poinsignon, C. Lattice vibrations of manganese oxides: Part I. Periodic structures. *Spectrochim. Acta Part A, Mol. Biomol. Spectrosc.* **2004**, *60*, 3, pp. 689–700. https://doi: 10.1016/S1386-1425(03)00279-8.
15. Bailey, M.R., Donne, S.W. Electrochemical impedance spectroscopy study into the effect of titanium dioxide added to the alkaline manganese dioxide cathode. *J. Electrochem. Soc.* **2011**, *158*, A802. https://doi 10.1149/1.3586045.
16. Ruetschi, P. Cation-vacancy model for MnO_2. *J. Electrochem. Soc.* **1984**, *131*, 2737. https://doi 10.1149/1.2115399.
17. Ruetschi, P. Influence of cation vacancies on the electrode potential of MnO_2. *J. Electrochem. Soc.* **1988**, *135*, 2657. https://doi 10.1149/1.2095405.
18. Ruetschi, P., Giovanoli, R. Cation vacancies in MnO_2 and their influence on electrochemical reactivity. *J. Electrochem. Soc.* **1988**, *135*, 2663. https://doi 10.1149/1.2095406.
19. Chabre, Y., Pannetier, J. Structural and electrochemical properties of the proton / γ-MnO_2 system. *Prog. Solid State Chem.* **1995**, *23*, 2737. https://doi.org/10.1016/0079-6786(94)00005-2.
20. Heuer, A.H., He, A.Q., Hughes, P.J., Feddrix, F.H. *ITE Lett. Batteries, New Technol. Med.* ***2000***, *1*, 926.
21. Donne, S.W., Lawrance, G.A., Swinkels, D.A.J. Redox processes at the manganese dioxide electrode: I. constant-current intermittent discharge. *J. Electrochem. Soc.* **1997**, *144*, 2949. https://doi 10.1149/1.1837942.
22. Iwamoto, M., Yoda, Y., Yamazoe, N., Seiyama, T. Study of metal oxide catalysts by temperature programmed desorption. 4. Oxygen adsorption on various metal oxides. *J. Phys. Chem.* **1978**, *82*, 2564–2570. https://doi.org/10.1021/j100513a006.